Correlation of stress corrosion cracking behaviour with electrical conductivity and open circuit potential in Al-Li-Cu-Mg-Zr alloys

K. S. Ghosh*, K. Das and U. K. Chatterjee

Studies of stress corrosion cracking (SCC) behaviour by slow strain rate test (SSRT), potentiodynamic electrochemical polarization and measurement of electrical resistivity were carried out on 8090 and 1441 Al-Li-Cu-Mg-Zr alloys in their peak aged T8, over aged T7 and retrogressed and reaged (RRA) T77 tempers. It has been found that the SCC resistance is maximum in the T7 temper, least in the T8 temper and in the RRA T77 tempers it lies in between to that of the T8 and T7 tempers, indicating that RRA heat treatment given to the T8 temper of both alloys caused an improvement of SCC resistance. Further, studies on the electrical conductivity measurements and electrochemical polarization of all tempers of both alloys showed that T7 temper has maximum electrical conductivity and most negative (anodic) open circuit potential (OCP), T8 has the minimum and the least respectively, whereas, in the T77 tempers these values lie in between to those of the T8 and T7 tempers. Therefore, a definite pattern of variation of these results with RRA treatment draws an attention to correlate SCC behaviour, electrical conductivity and OCP values which are explained on the basis of microstructural features revealed by TEM and XRD studies.

1 Introduction

Being lighter and having better stiffness, superior fatigue and creep crack growth resistance and better cryogenic toughness than those of the conventional aluminium alloys, Al-Li alloys are the obvious choice for aerospace industries. However, the peak strength Al-Li alloys have poor ductility, low fracture toughness, and are susceptible to environment-induced cracking (EIC) [1–3].

Generally, the high strength aluminum alloys are most susceptible to stress corrosion cracking (SCC) in the maximum strength peak aged T8 temper. Over aged temper T7 has an acceptable SCC resistance [4], but has lower strength. A novel heat treatment, retrogression and reaging (RRA) [5, 6], designated as T77 temper, combines the beneficial effects of both the T8 and T7 tempers [7]. RRA treatments result in approaching the microstructure to that of the T7 temper with an improved stress corrosion cracking resistance while retaining the T8 temper strength properties.

It has been reported in literature for the 7xxx series Al-Zn-Mg alloys [8, 9] that there is a strong relationship between stress corrosion resistance (SCC) and electrical conductivity and the same can be used as a measure of SCC resistance. *Islam* et al. [8] have concluded in their study on 7475 alloy that the SCC resistance increases with electrical conductivity. *Wallace* et al. [10] have also concluded that the SCC resistance of the 7075 aluminium alloy aged to or beyond T6 temper is proportional to the electrical conductivity of the material. In fact, studies on a wing lock attachment (WLA) fitting of an aircraft processed to the T73 condition was found to be virtually immune to SCC, and had much higher electrical conductivities. An important point is also mentioned that reaging the retrogressed state caused a further increase in conductivity of about 0.5% IACS, hence SCC resistance should be continually increasing during RRA. *Tsai* et al. [11] have attempted to find out whether any relationship exists between SCC resistance and electrical conductivity for all aging products in different aluminium alloys. They have found that the relation is valid only within the aging range from the peak aged to the over aged tempers and this relationship cannot be compared among different alloys and for different grain structures. Whether the relationship between electrical conductivity and SCC susceptibility also holds good in 8xxx series Al-Li alloys is not available in literature. Further, there is no reported work on the measurement of electrical conductivity values for the RRA tempers of the 8090 and 1441 Al-Li-Cu-Mg-Zr alloys.

Corrosion behaviour and electrochemical investigation were carried out on Al-Li alloys by several investigators [12–16]. The literature reveals that the electrochemical properties of the alloys depend primarily on the alloy composition and the nature, type, relative amounts and distribution of the micro-constituents in the alloy system which, in turn, are associated with the heat treatment i.e. aging temperature and time schedules. Environmental induced cracking (EIC) susceptibility of conventional aluminium alloys of various tempers has also been studied extensively [17–20], but no extensive discussion on the potential-SCC relationship has been dealt with in literature. The present work deals with the studies and discussion of SCC behaviour, measurement of electrical conductivity and open circuit potential (OCP) of the 8090 and 1441 Al-Li-Cu-Mg-Zr alloys of T8, T77 and T7 tempers and an indicative relationship among SCC resistance, electrical conductivity and open circuit potentials.

* *K.S. Ghosh*
Department of Metallurgical and Materials Engineering, National Institute of Technology, Warangal – 506 004 (India), E-mail: ksghosh2001@yahoo.co.uk, ghosh@nitw.ac.in

K. Das, U.K. Chatterjee
Department of Metallurgical and Materials Engineering, Indian Institute of Technology, Kharagpur – 721 302 (India)

Table 1. Chemical compositions (wt%) of the 8090 and 1441 Al-Li-Cu-Mg-Zr alloys

Alloy	Li	Cu	Mg	Zr	Fe	Si	Al
8090	2.29	1.24	0.82	0.12	0.09	0.044	Balance
1441	1.90	2.00	0.90	0.09	0.11	0.05	Balance

2 Experimental

The 8090 and 1441 (Russian grade) Al-Li-Cu-Mg-Zr alloys obtained from Defence Metallurgical Research Laboratory, Hyderabad, India, in sheet form have been used for the present studies. The chemical compositions (wt.%) of the 8090 and 1441 alloys are given in Table 1. The 8090 alloy sheet of 2.8 mm thickness was solutionised at 530–535 °C, water quenched, stretched 1.5–2.5%, followed by artificial aging at 170 °C for 24 h corresponding to the peak aged T8 temper, whereas the 1441 alloy sheet of 2 mm thickness was solutionized at 530–535 °C, water quenched, stretched by 1.5–2.5%, followed by duplex artificial aging at 150 °C for 4 h and then 170 °C for 24 h to the T8 temper. The 8090 and 1441 alloy sheets were aged at 170 °C for about 120 h to obtain the over aged T7 temper. The triplanar optical micrographs of the alloys of T8 tempers are shown in Fig. 1(a–b). Fig. 1a, microstructure of the 8090 alloy exhibits the grains are equiaxed in the longitudinal (L) direction, but highly flattened and elongated in the long transverse (LT) as well as in the short transverse (ST) directions as a consequence of deformation induced during rolling operation. Thus, the transverse grains appear to have a large aspect ratio; whereas the microstructure of the 1441 alloy (Fig. 1b) shows the grains are more or less equiaxed in all the three directions. The average grain sizes in longitudinal direction of the 8090 and 1441 alloys have found to be 10–15 μm and 15–20 μm, respectively.

The 8090 and 1441 alloys in the T8 tempers were subjected to retrogression and reaging (RRA) treatments. The schedules of the RRA treatments applied to the T8 tempered alloys are stated in Table 2. RRA treatments were carried out in a small vertical tube furnace in air maintaining the temperature within $\pm$ 2 °C. The process of retrogression involved the heating up of the specimens for a short duration at temperatures above and below the δ' solidus line of the Al-Li system, cooling in ice cold water followed by immediate isothermal or duplex reaging to peak aged temper condition. Thus the total aging time of the RRA T77 tempers is more than twice to that of the conventional T8 temper. However, the aging time of the T7 temper is about four times to that of T8 temper.

Tensile specimens, transverse to the rolling direction (unless otherwise specified) were obtained from both the 8090 and 1441 alloy sheets for SCC studies. The dimensions of the tensile specimens for the 8090 alloy were 25 mm extended gauge length, 4 mm width and 2.6 mm thickness and for the 1441 alloy it was 20 mm extended gauge length, 4 mm width and 1.8 mm thickness. Coupons of dimensions 10 mm length and 10 mm wide were used for electrochemical potentiodynamic polarization studies. The gauge portion of all the tensile specimens and surfaces of the coupons were ground to 100 μm minimum from the original sheet thickness to remove the lithium and magnesium depleted surface and sub-surface zones developed during heat treatments in air [21]. The specimens were wet polished in kerosene up to 600 grits and finally deoiled before testing.

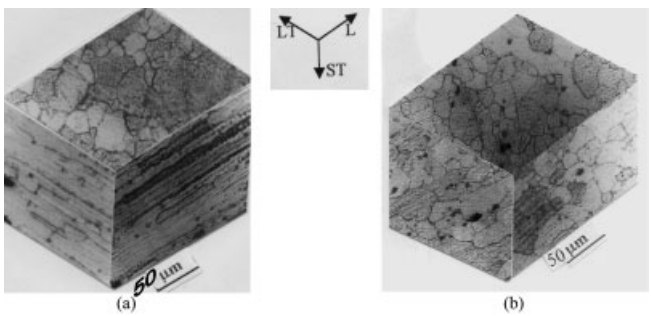

Fig. 1. Triplanar optical micrographs of the as-received (a) 8090-T8 and (b) 1441-T8 alloys

Table 2. Retrogression and reaging schedules adapted to the 8090 and 1441 alloys

Alloy	Retrogression temperature and time	Reaging schedule	RRA Temper Designation
8090-T8	At 280 °C for 8 min.	Isothermal reaging at 170 °C for 24 h	8090R280IA
		Duplex reaging at 150 °C for 36 h, followed by heating to 190 °C at a rate of 5–7 °C/min and holding for 1 h at the temperature	8090R280DA
		Isothermal reaging at 170 °C for 24 h	8090R250IA
	At 250 °C for 12 min.	Duplex reaging at 150 °C for 36 h, followed by heating to 190 °C at a rate of 5–7 °C/min and holding for 1 h at the temperature	8090R250DA
1441-T8	At 270 °C for 5 min.	Isothermal reaging at 170 °C for 26 h	1441R270IA
		Duplex reaging at 150 °C for 36 h, followed by heating to 190 °C at a rate of 5–7 °C/min and holding for 1 h at the temperature	1441R270DA
		Isothermal reaging to peak aged temper i.e. at 170 °C for 26 h	1441R230IA
	At 230 °C for 15 min.	Duplex reaging (DA) at 150 °C for 36 h, followed by heating to 190 °C at a rate of 5–7 °C/min and holding for 1 h at the temperature	1441R230DA

Microstructural features of the T8, RRA and T7 tempers were observed by XRD and TEM studies. X-ray diffraction was taken using a Philips PW 1710 diffractometer unit with cobalt as well as copper targets. TEM samples were prepared by mechanically thinning to a thickness of approximately 100 μm, and finally thinning down to perforation using a Fischione twin-jet electropolisher, operating at 25 volts and 2.5 amps current, in an electrolyte of composition 30% HNO_3 and 70% CH_3COOH at a temperature of approximately $-$ 20 °C.

Stress corrosion cracking (SCC) studies were performed by slow strain rate test (SSRT) under total immersion condition in 3.5% NaCl + 0.1M LiCl + 0.7% H_2O_2 solution. SSRT test was performed using a CORTEST unit at an initial strain

rate of $6 \cdot 10^{-6}$ s^{-1} and $5.5 \cdot 10^{-6}$ s^{-1} for the 8090 and 1441 alloys, respectively. Tests were repeated at least thrice to confirm the results. The SCC susceptibility was expressed by the parameter of ductility ratio (DR) defined as the ratio of plastic strain to fracture in environment (ε_{envn}) to that in air (ε_{air}) i.e. $\varepsilon_{envn}/\varepsilon_{air}$.

In resistivity measurements, the four-probe method was adopted. A constant current was fed from one end to the other end of the rectangular sample and the voltage was measured across two contacts, which were away from the current contacts in order to keep the lines of current flow uniform and parallel. A constant current was supplied by a Shenzhen Mastech DC power supply unit and the voltage drop was measured across the contacts of fixed length using a Keithley 177 Microvolt DMM unit. The resistivity of the sample was calculated from the voltage drop, the applied current, and the geometry of the samples.

Potentiodynamic electrochemical polarisations were carried out, by using a computer controlled Meinsberger potentiostat/galvanostat with built-in PS6 software. Experiments were conducted using the standard three electrodes configuration: saturated calomel electrode as a reference and platinum electrode as counter and the sample as the working electrode. Specimens were immersed in 3.5% NaCl + 0.1M LiCl + 0.7% H_2O_2 solution and the polarization scan was carried out towards more noble values at a scan rate of 0.5 mV/sec, after allowing a steady state potential to establish.

3 Results

Fig. 2(a–b) shows the X-ray diffractograms of the 8090 and 1441 alloys in the T8 and RRA tempers. The diffractograms of the T8 and RRA tempers of the alloys, show the peaks of all the probable phases, such as α-Al matrix, δ' (Al_3Li), δ (AlLi), S' (Al_2CuMg), T_1 (Al_2CuLi) and β' (Al_3Zr) phases that would be present in the alloy system [22]. The diffractograms of the RRA tempers exhibit an additional $T_{1(102)}$ peak and other intensified peaks of the T_1 and δ phases compared with the exhibited peaks in the 8090-T8 and 1441-T8 tempers. Thus, RRA treatments resulted in the formation of more amounts of T_1 and δ phases. The effect of RRA treatment on the S' phase could not be analyzed with the XRD peaks as the peaks of this phase overlap with the α-Al matrix peaks. However, DSC and TEM studies could explain the effect and has been explained elsewhere by the authors [23, 24].

A few representative TEM photomicrographs of both the 8090 and 1441 alloys of the T8 and RRA tempers are given in Fig. 3(a–h). Fig. 3a, the TEM photomicrograph of the 8090-T8 alloy temper, exhibits numerous coherent β' (Al_3Zr) precipitates. Due to its stability, the size and distribution of these β' particles do not alter upon RRA treatment and aging treatment. Fig. 3b, the TEM bright field image of the 1441-T8 temper, shows a uniform distribution of fine T_1 and S' phases within the matrix and equilibrium δ phase at the grain boundaries. In one of the grains, the preferential heterogeneous precipitation of these phases along the dislocations is also observed. Figs. 3c and 3d show the dislocation structure within the grain and subgrains of the 8090-T8 and 8090R280IA RRA tempers, respectively. Fig. 3d, TEM photomicrograph of the 8090R280IA RRA temper, shows a decrease in dislocation density in the grains compared to the dislocation density in the T8 temper (Fig. 3c). This is due to the retrogression treatment at 280 °C annihilates dislocations of opposite signs. Thus, retrogression treatment results in a decreased dislocation density. Similar observations are also reported in literature [22, 23]. Fig. 3e, for the 8090R280IA temper, shows the equilibrium δ phase at the high angle grain boundaries as well on the subgrain boundaries. RRA treatment results in the formation of more amounts of δ and coarsening of the precipitates along grain and subgrain boundaries and similar observations are reported in literature for alumimium base alloys [18, 25, 26]. Fig. 3f, TEM photomicrograph of the 8090R280DA RRA temper, displays uniform heterogeneous rodlike and platelike (i.e. impinged rectangular rods along a line) S' and T_1 precipitates. Fig. 3g, TEM micrograph of the 1441R230DA RRA temper, shows the equilibrium δ phase at the high angle grain boundaries and at higher magnification this equilibrium phase is also seen at the sub-grain boundaries (Fig. 3h). The enhanced precipitation of equilibrium δ phase of the RRA tempers is because of more aging time in the RRA temper. The higher the aging time the greater is the nucleation and growth of δ phase and the transformation of δ' (Al_3Li) phase to δ (AlLi) as well.

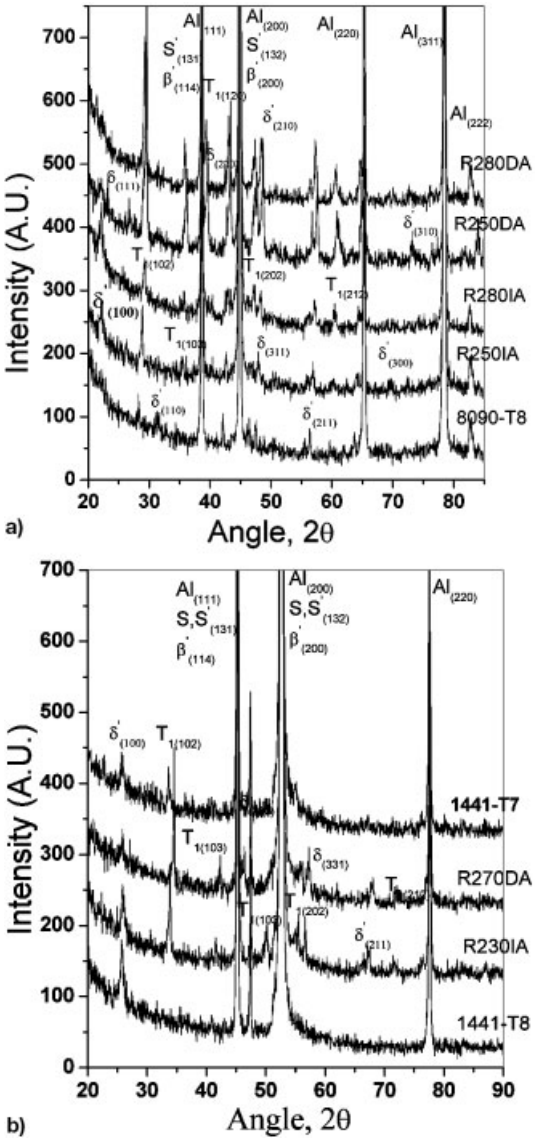

Fig. 2a. XRD of the 8090 alloy of various tempers using CuK_α radiation

Fig. 2b. XRD of the 1441 alloy of various tempers using CoK_α radiation

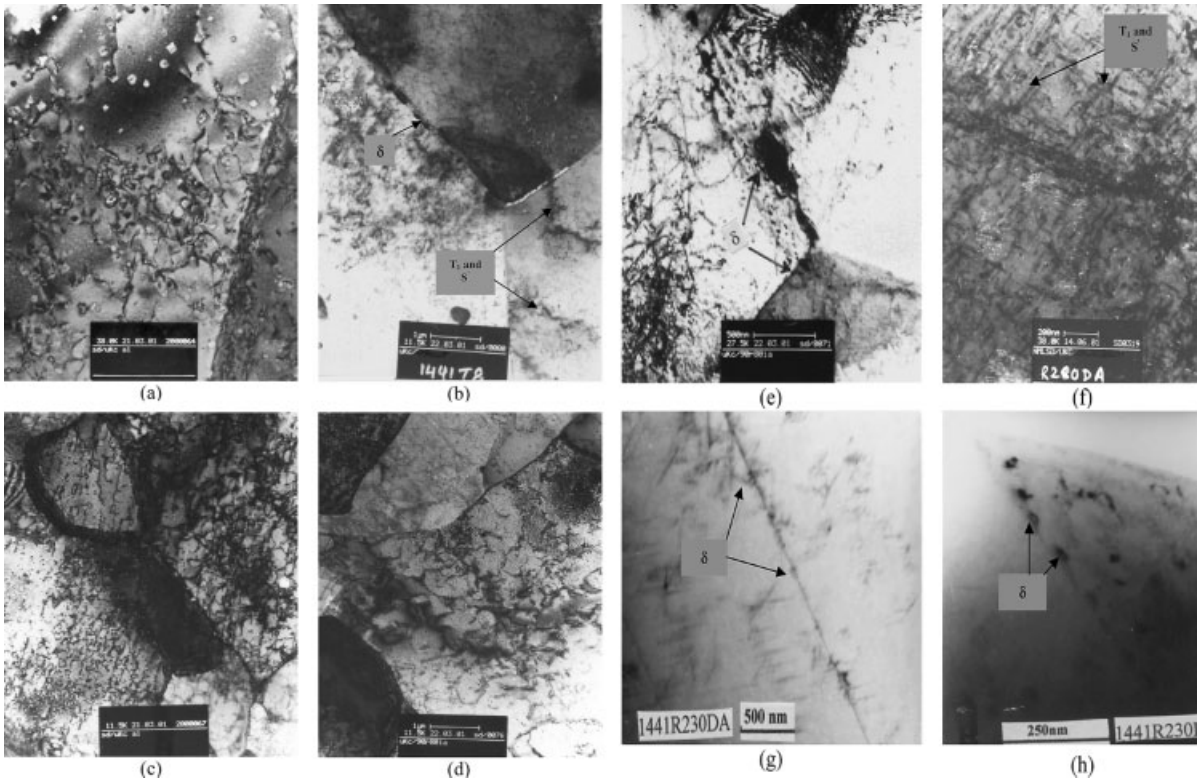

Fig. 3(a–h). TEM photomicrographs of (a) 8090-T8 temper showing β' precipitates within the grain as well as on the dislocations, (b) 1441-T8 temper exhibiting homogeneous distribution of T_1 and S′ precipitates and heterogeneous precipitation of T_1 and S′ on dislocations, (c) 8090-T8 temper displays dislocation densities, (d) 8090R280IA RRA temper shows low dislocation densities, (e) 8090R280IA RRA temper shows equilibrium δ precipitation along the grain and sub-grain boundaries, (f) 8090R280DA RRA temper displays uniform distribution of S′ and T_1 precipitates, (g) 1441R230DA RRA temper exhibits equilibrium δ precipitates at the grain boundary and at higher magnification, (h) δ phase is also revealed at the subgrain boundaries

Fig. 4(a–d) shows the representative stress strain curves of the 8090 alloy of the 8090-T8, 8090R250IA, 8090R280IA, and 8090-T7 tempers in air and in 3.5% NaCl + 0.1 M LiCl + 0.7% H_2O_2 solution. Similarly, Fig. 5(a–d) shows the representative stress strain curves of the 1441 alloy of T8, 1441R270DA, 1441R230DA and T7 tempers in air and in 3.5% NaCl + 0.1 M LiCl + 0.7% H_2O_2 solution. The curves show that 3.5% NaCl + 0.1 M LiCl + 0.7% H_2O_2 environment causes a drastic reduction of plastic strain to fracture for all the tempers i.e. T8, RRA T77 and T7 tempers, indicating that all the alloy tempers are susceptible to SCC in the medium. However, for both the alloys, the reduction of plastic strain to fracture is maximum in the T8 temper, least in the T7 and in the RRA tempers it is intermediate of the T8 and T7 tempers. Therefore, it can be concluded that the RRA treatments given to the T8 tempers of the alloys cause an improvement of SCC resistance.

Fig. 6(a–b), bar diagram, shows the plastic strain to fracture of the 8090 and 1441 alloys of various tempers tested in air and in 3.5% NaCl + 0.1 M LiCl + 0.7% H_2O_2 solution. Ductility ratio (DR) of the respective tempers is also indicated in the bar diagram. The bar diagram shows that the T7 temper has the maximum ductility ratio (DR), the T8 temper has the least, whereas the ductility ratio (DR) values of the RRA tempers are in between to that of the T8 and T7 tempers. Therefore, the T7 temper exhibits maximum resistance to SCC, T8 temper is the minimum and the SCC resistance of the RRA T77 tempers is intermediate to that of the T7 and T8 tempers. Thus, the RRA treatment applied to the T8 temper has resulted in an improvement of SCC resistance. The possible SCC mechanism in the T8 temper and the higher SCC resistance in the T7 and T77 tempers compared to the T8 temper is explained in the subsequent discussion section.

Fig. 7(a–b) shows the potentiodynamic polarization curves of the 8090 and 1441 alloys of various tempers in 3.5% NaCl + 0.1M LiCl + 0.7% H_2O_2 solution. The shape of the polarization curves is similar for all the tempers. The cathodic currents in the cathodic overvoltage region are more or less the same in all the tempers, and this is so with the anodic current in the anodic overvoltage region. But the curves show that the open circuit potential (OCP) has shifted towards more negative values (anodic) with the RRA and with the aging time. Thus, the OCP of the over aged temper has the most negative value, whereas the OCP values of the retrogressed and reaged tempers lie in between the OCP values of the over aged and peak aged tempers. The trends of variation of electrochemical behaviour with the aging time of these tempers in our studies on the 8090 and 1441 alloys are consistent with the reported results in literature [27–29].

Tables 3a and 3b give the electrical conductivity values and open circuit potentials (OCP) obtained from potentiodynamic polarization studies in 3.5% NaCl + 0.1M LiCl + 0.7% H_2O_2 solution of the 8090 and 1441 alloys in their T8, RRA and T7 tempers. The SCC susceptibility index values viz. the ductility ratio (DR) in 3.5% NaCl + 0.1M LiCl + 0.7% H_2O_2 solution of all these tempers of the alloys, are also incorporated in the tables for the sake of a quick comparison.

The electrical conductivity values of all the tempers are in the range of the reported values of the Al-Li-Cu-Mg-Zr alloy series [1]. The conductivity values have increased with in-

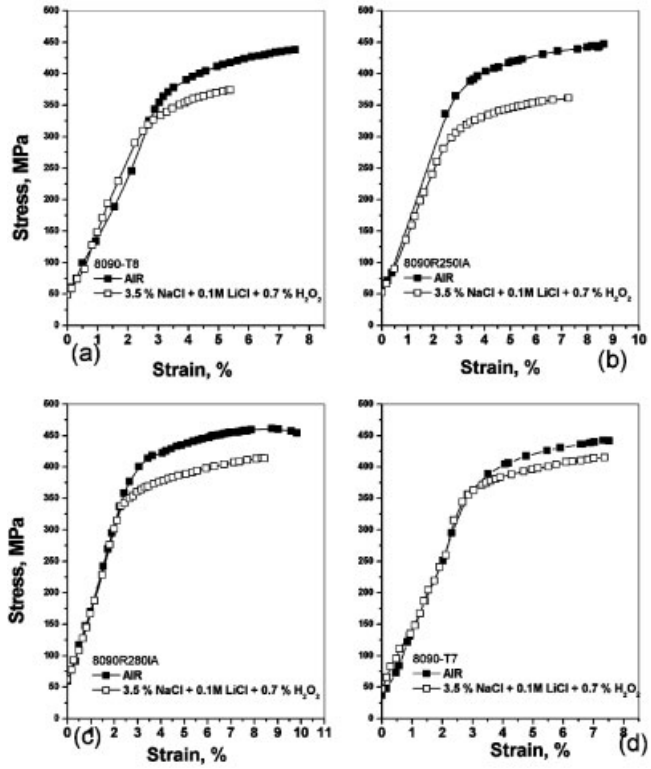

Fig. 4. Representative stress strain curves of (a) 8090-T8, (b) 8090R250IA, (c) 8090R280IA and (d) 8090-T7 tempers tested at a strain rate of $6.0 \cdot 10^{-6}$ s^{-1} in air and in 3.5% NaCl + 0.1M LiCl + 0.7% H_2O_2 solution

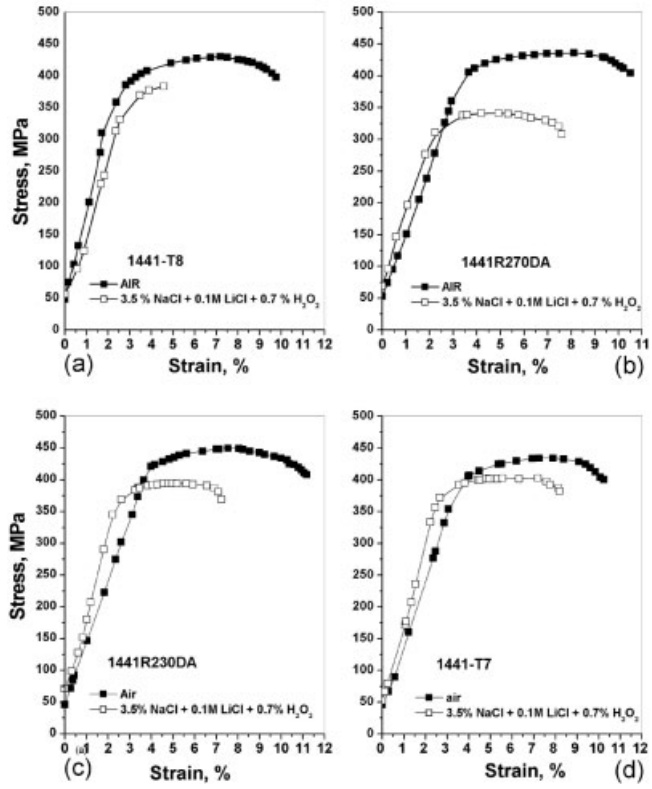

Fig. 5. Representative stress strain curves of (a) 1441-T8, (b) 1441R270DA, (c) 144R230Da and (d) 1441-T7 tempers tested at a strain rate of $5.5 \cdot 10^{-6}$ s^{-1} in air and in 3.5% NaCl + 0.1M LiCl + 0.7% H_2O_2 solution

crease in aging time. The T7 temper has the highest conductivity and peak aged temper has the lowest for both the alloys. The conductivity values of the RRA tempers lie in between the conductivity values of the T8 and T7 tempers. Thus, it can be stated that the RRA treatment of T8 temper causes an increase in electrical conductivity.

4 Discussion

The presence of small amounts of LiCl and H_2O_2 in the 3.5% NaCl solution makes the media susceptible to SCC for the alloy system under total immersion condition by maintaining a condition of borderline passivity essentially required for the SCC process [30–32] as compared to that in only 3.5% NaCl solution because of its strong depassivating nature. The applied stress during slow strain rate tests (SSRT) assists rupturing the passive film and leads to the local dissolution of the exposed area as it acts as a small anode in contact with a large cathode i.e. the film surface. The film rupture exposes an area containing precipitates and precipitate free zones that are electrochemically different providing local galvanic cells.

The microstructure of the conventional T8 temper comprises a combination of δ' (Al_3Li), S′ (Al_2CuMg), T_1 (Al_2CuLi) and β' (Al_3Zr) phases homogeneously and heterogeneously precipitated within the matrix, and δ (AlLi), T_1 (Al_2CuLi) and β' (Al_3Zr) phases at the grain boundaries (Fig. 3).

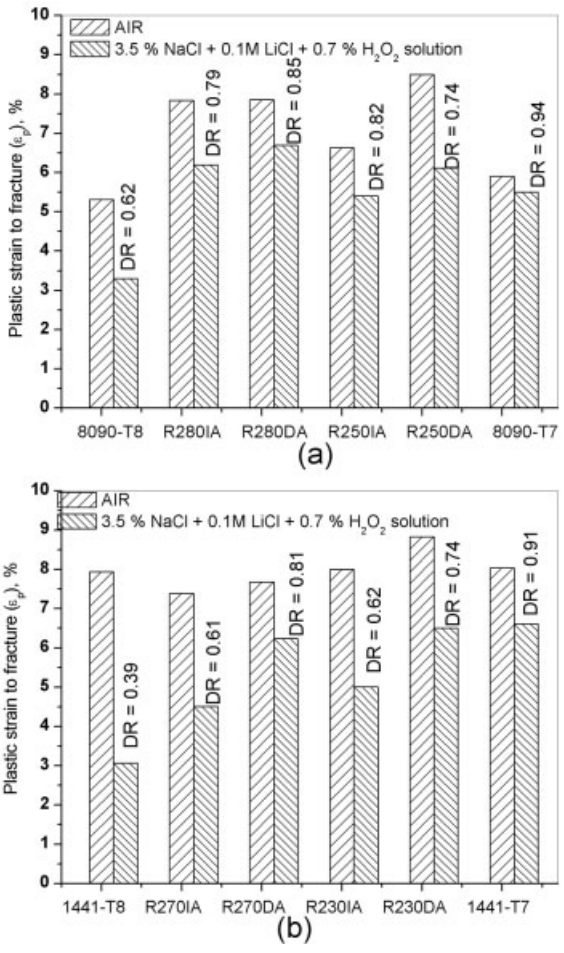

Fig. 6. Plastic strain to fracture of the alloys (a) 8090 and (b) 1441 of various tempers

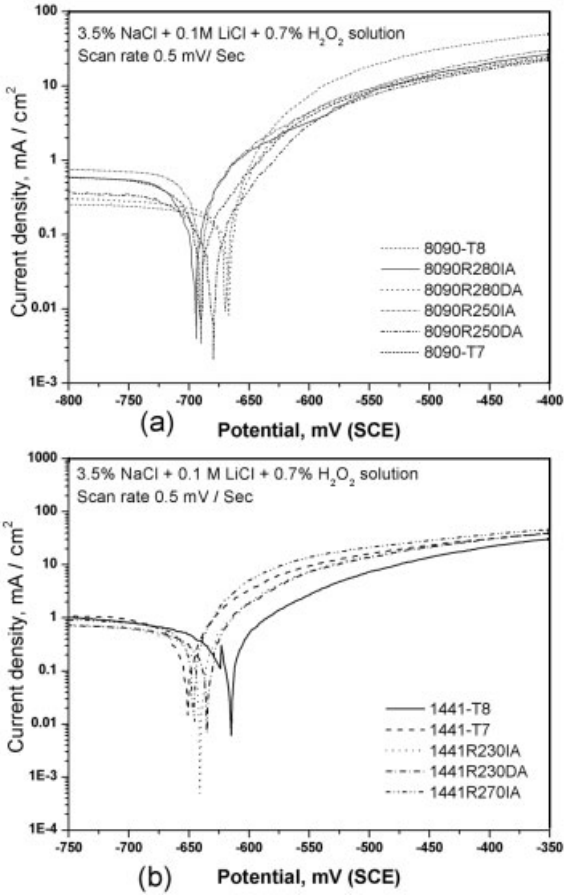

Fig. 7. Potentiodynamic polarisation curves of the alloys (a) 8090 and (b) 1441 of various tempers

The initiation of SC cracks in this case is caused by the preferential dissolution of the anodic grain boundary and sub-grain boundary δ and T_1 precipitate forming a lots of galvanic cells. The crack initiation is assisted by the propensity for coarse planar slip generated due to the coherent δ' precipitates which causes stress concentration at the grain boundaries. It is well known that SCC of aluminium alloys follows intergranular paths with very few exceptions [33]. *Lumsden* et al. [34] stated that the presence of precipitates in grain boundaries supports anodic dissolution in the 8090 alloy more strongly than other models. *Conde* et al. [35] showed the fractographs containing intense attack, a consequence of the preferential dissolution of grain boundary precipitates and the areas present with microvoids that are due to intense intergranular attack, and not a consequence of ductile fracture. The nucleation of cracks has also been reported to take place by the pit formation inside which the solution pH goes down to the level of 3–4 [4, 19]. Fig. 8(a–c) shows that the crack has initiated from the base of the pit as well as from the other sites e.g. intergranularly and anodically dissolved zone, which resulted from the dissolution of anodic phases. Thus an anodic dissolution promoted intergranular SCC mechanism seems to be operative in the alloy, and intergranular cracking is evident in Fig. 8c.

The SCC process in the RRA tempers is believed to be the same as that in the T8 temper of both the alloys. But, the improvement of SCC resistance in the RRA tempers compared to the T8 tempers of the alloys can largely be explained on the basis of the microstructural changes upon RRA heat treatment mainly in regard to the size and distribution of the anodic

Table 3a. Electrical conductivity, OCP values and SCC susceptibility index of the 8090 alloy of various tempers

Alloy Temper	Electrical Conductivity X 10^6/ (mho cm^{-1}) (IACS)	OCP, mV (SCE) in 3.5% NaCl + 0.M LiCl + 0.7% H_2O_2 solution	DR ($\varepsilon_{envn}/\varepsilon_{air}$) in 3.5% NaCl + 0.1M LiCl + 0.7% H_2O_2 solution
8090-T8 (L)	0.1132 (19.25)	–	–
8090-T8 (LT)	0.0942 (16.02)	− 670	0.62
8090R250IA	0.1101 (18.73)	− 694	0.82
8090R250DA	0.1069 (18.18)	− 667	0.74
8090R280IA	0.1098 (18.67)	− 690	0.79
8090R280DA	0.1071 (18.21)	− 680	0.85
8090-T7	0.1222 (20.78)	− 693	0.94

IACS: International Annealed Copper Standard.

Table 3b. Electrical conductivity, OCP values and SCC susceptibility index of the 1441 alloy of various tempers

Alloy Temper	Electrical Conductivity X 10^6/ (mho cm^{-1}) (IACS)	OCP, mV (SCE) in 3.5% NaCl + 0.M LiCl + 0.7% H_2O_2 solution	DR ($\varepsilon_{envn}/\varepsilon_{air}$) in 3.5% NaCl + 0.M LiCl + 0.7% H_2O_2 solution
1441-T8	0.1050, (17.85)	− 615	0.39
1441R230IA	0.1074, (18.27)	− 630	0.62
1441R230DA	0.1067, (18.15)	− 627	0.74
1441R270IA	0.1078, (18.33)	− 641	0.61
1441R270DA	0.1085, (18.44)	− 635	0.81
1441-T7	0.1138, (19.35)	− 646	0.91

IACS: International Annealed Copper Standard.

phases, notably δ (AlLi) and T_1 (Al_2CuLi), precipitated within the grains, along the subgrain boundaries and the grain boundaries.

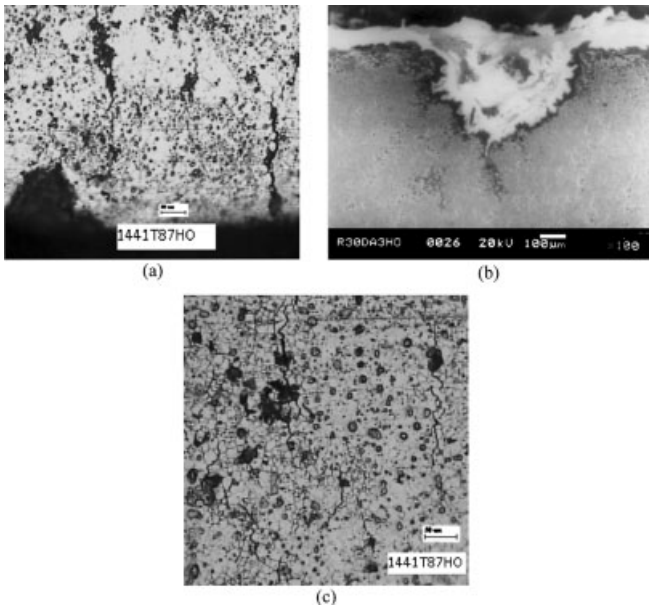

Fig. 8(a–c). SC cracks in 3.5% NaCl + 0.1M LiCl + 0.7% H_2O_2 solution: (a) 1441-T8 temper crack initiation from the base of the pit as well as from the intergranularly and anodically denuded/dissolved region, (b) 1441R230DA temper cracking from the base of the pit and (c) crack propagation path is intergranular

RRA treatments have resulted in the formation of additional equilibrium δ (AlLi) and T_1 phases (Figs. 2 and 3). Thus, in the RRA tempers, the widespread dispersion of T_1 and δ phases throughout the matrix, along the grain boundaries as well as on the sub-grain boundaries, reduces the potential difference for the formation of microscopic galvanic cells. Therefore, the tendency of uniform corrosion/attack is more, whereas the propensity of intergranular dissolution is largely reduced resulting in an improvement of resistance to SC crack initiation and propagation. Further, RRA treatment decreases the dislocation density, as found by the authors [23] and others [22, 36, 37]. The lower dislocation density reduces the stress factor for SCC process resulting in an improvement of SCC resistance. Again, in the RRA tempers, the stress intensity/factor will be less intense because of more and widespread uniform distribution of S′ phase throughout the matrix that promotes cross slip resulting in the minimization of planar slip [23]. Therefore, all these factors cause an improvement of SCC resistance in the RRA tempers compared to that of the peak aged T8 temper. In the over aged temper, the aging time is much longer compared to the peak aged and retrogressed and reaged temper. The more the aging time, the more is the precipitation of δ and T_1 phases, at the grain boundaries and the sub-grain boundaries. Therefore, the attack is more uniform with a low propensity of intergranular corrosion, leading to an improved SCC resistance [18, 38].

From the electrical conductivity values of both the alloys the following observations could be made:

- The conductivity values of all the tempers are in the range of the reported values of the 8xxx alloy series.
- For the 8090 alloy of the T8 temper, electrical conductivity value is higher in the longitudinal (L) direction than that in the long transverse (LT) direction.
- The over aged temper has the highest conductivity whereas the conductivity value of the peak aged temper is the least. Hence, conductivity values have increased with the increase of aging time.
- The conductivity values of the RRA tempers of both the alloys lie in between the conductivity values of the T8 and T7 tempers.

The conductivity of metallic materials at a given temperature depends on the grain structure, the solute content, second phase precipitates, segregation, vacancies, imperfections etc. According to the *additivity rule of Mattheissen*, the electrical resistivity is given by the following relation.

$$\rho_t = \rho_T + \rho_r \quad (1)$$

where ρ_t is the total resistivity, ρ_T is the thermal part of the resistivity and ρ_r is the residual resistivity.

For a given temperature (in our studies electrical resistivity values are measured at room temperature), ρ_T, arising due to phonon scattering remains same for samples of various alloy tempers and thus the total resistivity depends only on the residual resistivity.

The residual resistivity of the alloys is primarily controlled by the interaction of the moving electrons (under an applied electric field) available in the conduction bands with the localized strain fields in the crystalline matrix. These localized strain fields provide scattering centers for the moving electrons. Thus, the residual resistivity is attributable to the scattering centers arising from the solutes, the impurities, the size and distribution of second phase precipitates and also from the dislocations. A decrease in scattering centers will lead to an increase in electrical conductivity. Further, for a given alloy composition, the amount of impurities and the solute contents remain same, but the size and the distribution of the second phase precipitates as well as the dislocation density that vary with the aging time and RRA treatments, would have an influence on the electrical conductivity values. Thus, the RRA tempers with low dislocation densities as compared to the as-received T8 temper (Figs. 3c and 3d) [22, 23, 36, 37] have higher electrical conductivity values with respect to the T8 temper and this is because of the less scattering centers that arise from dislocations to the moving electrons.

The variation of electrical conductivity values could also be attributed to the alteration of the precipitate size, their distribution and morphology upon RRA and aging treatments. Since, the 8090 and 1441 alloy systems comprise a large number of precipitates such as δ', S′, T_1 and β' precipitated homogeneously and heterogeneously within the matrix, and equilibrium δ, T_1 and β' (Al_3Zr) phase formed at the grain boundaries as well, it is very difficult to pinpoint the role of each and every precipitate on the observed variation of the electrical conductivity values of the RRA and T7 tempers. The alternation of microstructural features upon RRA treatment in the 8090 alloy has been discussed elsewhere [23]. It has been highlighted that RRA treatment and aging time would not alter the size, relative amounts and distribution of the β' (Al_3Zr) due to its high stability. Analysis of δ' particles size and their distribution of T8 and RRA tempers of both the alloys using Leica QWIN software revealed no appreciable variation of mean particle diameter and volume fractions. This is expected, otherwise an equivalent hardness and strength properties of T8 and RRA tempers would not have been obtained [24]. But, in the T7 tempers the relative amount of δ' particles and its size have a role in the electrical conductivity value. It is a well established fact that 8–10% lower strength of the T7 temper compared to that of the T8 temper in all aluminium alloys is attributed to the larger size of the δ' particles. The larger the δ' precipitates size the fewer will be the number that results in lower electron scattering centers accounting for an increase of electrical conductivity. Hence, the electrical conductivity value in the T7 temper is maximum. Since, there is an observation of higher electrical conductivity values and improved SCC resistance in the RRA tempers and in the over aged tempers compared to that of the T8 tempers of both the alloys, an inference could be drawn that the higher the electrical conductivity the higher would be the SCC resistance.

Figs. 7a and 7b, the potentiodynamic polarisation curves of the 8090 and 1441 of various tempers, show that the OCP has shifted to more negative values with aging time and RRA treatment. Similar trends have also been observed by other researchers [27]. The OCP value of the over aged temper has the most negative value, whereas the OCP values of the retrogressed and reaged tempers lie in between the OCP values of the over aged and peak aged tempers. It is an established fact that in a given environment the OCP of an alloy depends on the microstructure and the constituent phases present in the system. In these 8090 and 1441 Al-Li-Cu-Mg-Zr alloy systems phases such as δ, T_1 and S′ are anodic in nature [15, 28, 39]. Thus, the more negative values of OCP values (i.e. the shifting of OCP towards more negative direction) of the RRA tempers compared to those in the T8 tempers for both the alloys are attributed to the presence of higher amounts of these phases, which is evident from Figs. 2 and 3. The more the aging time (i.e. for the T7 and RRA tempers compared to T8 tempers for both the alloys), there will be higher amounts of precipitation of the anodic phases, especially equilibrium δ phases at the grain bound-

aries, sub-grain boundaries as well as within the grains. The higher amounts of δ phase at the grain boundaries, sub-grain boundaries as well as within the grains would enhance uniform attack, but minimize localized intergranular attack and thereby cause an improvement of SCC resistance. Thus, the presence of higher amounts of equilibrium δ phases will shift the OCP values towards more negative direction and simultaneously enhance the resistance to SCC. Hence, it could be stated that the more negative the OCP values are, the higher will be the SCC resistance.

5 Conclusions

1. XRD and TEM studies exhibited all the probable phases such as α-Al matrix, δ', δ, S′, T_1 and β' phases that would be present in the alloy system. The diffractograms of the RRA tempers exhibited additional $T_{1(102)}$ peak and other intensified peaks of the T_1 and δ phases, indicating that RRA treatments resulted in the formation of more amounts of these phases. TEM photomicrographs of the RRA tempers showed a decrease of dislocation densities compared to that of the T8 temper. Further, TEM photomicrographs of the RRA tempers for both the alloys have exhibited enhanced precipitations of equilibrium δ phase.
2. Both SCC resistance and electrical conductivity values of the 8090 and 1441 alloys are lowest in the T8 temper, highest in the T7 temper and intermediate in the RRA tempers. The OCP value of the T7 temper has the most negative value, whereas for the RRA tempers it lies in between to that of the T7 and T8 tempers. The increased electrical conductivity value in the RRA tempers is due to the decrease of dislocation densities and alteration of microstrucrutal features upon RRA treatment. The higher resistance to SCC in the RRA and T7 tempers is because of lower dislocation densities enabling a reduced stress factor for the SCC process and enhanced precipitation of equilibrium δ phase which minimizes the intensity of intergranular corrosion. The shifting of OCP values towards more negative (i.e. anodic) direction of the RRA and T7 tempers is attributed to the enhanced precipitation of anodic δ, T_1 and S′ phases.
3. A correlation is evident that the higher the electrical conductivity value and the more negative the value of OCP, the higher is the SCC resistance of the alloys.

6 Acknowledgement

The authors would like to thank Dr. *A. A. Gokhale* and Dr. *Vijaya Singh*, Scientists, Defence Metallurgical Research Laboratory, Hyderabad, India, for providing alloys. Authors also thank to Mr. *Samar Das*, National Metallurgical Laboratory, Jamshedpur for carrying out TEM studies.

7 References

[1] *ASM Specialty Handbook, Aluminum and Aluminum Alloys*, eds. J. R. Davis, Davis & Associates, ASM International, The Materials Information Society, Ohio, **1998**.
[2] S. J. Harris, B. Noble, K. Dinsdale, T. H. Sanders Jr. and E. A. Starke Jr. (Eds.), *Proc. 2nd Int. Conf. Aluminium Lithium Alloys*, TMS, AIME, Warrendale, PA, **1983**, pp. 219–235.
[3] L. Christodoulou, L. Struble, J. R. Pickens, ibid, pp 561–579.
[4] N. J. H. Holroyd, A. Gray, G. M. Scamans, R. Hermann, C. Baker, P. J. Gregson, S. J. Harris and C. J. Peel (Eds.), *Proc. 3rd Int. Conf. on Aluminium Lithium Alloys III*. The Institute of Metals of London, **1986**, pp. 310–320.
[5] B. Cina, *US Patent No. 3856584*, December 24, **1974**.
[6] B. Cina, B. Ranish, Paper No. XXV, *Aluminium Industrial Products*, ASM, Pittsburg, PA, October, **1974**.
[7] B. S. Kaneko, *Metal Progress* **1980**, *41*, 41.
[8] M. U. Islam, W. Wallace, *Metal Technology* **1983**, *10*, 386.
[9] T. Ohnishi, H. Shiota, *J. Japan Inst. Light Met.* **1986**, *36*, 667.
[10] W. Wallace, J. C Beddoes, M. C. deMatherbe, *Canadian Aeronautics and Space Journal* **1981**, *27*, 222.
[11] T. C. Tsai, T. H. Chung, *Corrosion* **1996**, *52*, 414.
[12] A. Roth, H. Kaesche, *Advanced Materials & Processes* **1992**, *6*, 1197.
[13] A. Roth, H. Kaesche, ibid, **1992**, *6*, 1207.
[14] J. M. Sater, T. H. Sanders, T. H. Sanders Jr., and E. A. Starke Jr., (Eds.), *Proc. 5th Int. Conf. Aluminium Lithium Alloys*, Materials and Component Engineering Publications (MCEP), Warrendale, PA, **1989**, pp. 1217–1226.
[15] B. Bavarian, J. Becker, S. N. Parikh, M. Zamanzadeh, ibid, **1989**, pp 1227–1236.
[16] E. L. Colvin, S. J. Murtha, ibid, **1989**, pp 1251–1260.
[17] P. L. Plane, J. A. Gray, C. T. E. Smith, C. Baker, P. J. Gregson, S. J. Harris and C. J. Peel (Eds.), *Proc. 3rd Int. Conf. Aluminium Lithium Alloys in Aluminum- Lithium Alloys III*, , The Inst. Metals, London, **1986**, pp 273–281.
[18] A. Gray, N. L. H. Holroyd, J. White, T. H. Sanders Jr., and E. A. Starke Jr.,(Eds.) *Proc. 5th Int. Conf. Aluminium Lithium Alloys*, Materials and Component Engineering Publications (MCEP), Warrendale, PA, **1989**, pp. 1175–1186.
[19] M. Ahmad, G. Champier, B. Dubost, D. Miannay and L. Sabetay, (Eds.), *Proc. 4th Int. Conf. Aluminium Lithium Alloys, J. Phys.*, Suppl. **1987**, *48*, pp. C3:871–C3:879.
[20] R. C. Dorward, K. R. Hasse, *Corrosion*, **1987**, *43*, 408.
[21] S. Fox, H. M. Flower, D. C. McDarmaid, C. Baker, P. J. Gregson, S. J. Harris and C. J. Peel (Eds.), *Proc. 3rd Int. Conf. Aluminium Lithium Alloys*, **1986**, pp. 263–272.
[22] V. Komisarov, M. Talianker, B. Cina, *Mat. Sci. & Engg.* **1998**, *A242*, 39.
[23] K. S. Ghosh, K. Das, U. K. Chatterjee, *Mat. Sci and Tech.* **2004**, *20*, 825.
[24] K. S. Ghosh, K. Das, U. K. Chatterjee, *Metallurgical and Mater Trans A* **2004**, *35A*, 3681.
[25] V. Komisarov, M. Talianker, B. Cina, *Mat. Sci. & Engg.* **1996**, *A221*, 113.
[26] J. K. Park, *Mat. Sci. & Engg.* **1998**, *A103*, 223.
[27] A. Gray, G. Champier, B. Dubost, D. Miannay and L. Sabetay (Eds.), *Proc. 4th Int. Conf. Aluminum Lithium, J. Phys.* **1987**, *48*, pp. C3: 891–C3:904.
[28] M. Reboul, P. Meyer, ibid, C3:881–C3:889.
[29] J. M. Sater, T. H. Sanders, T. H. Sanders Jr. and E. A. Starke Jr. (Eds.), *Proc. 5th Int. Conf. on Aluminium Lithium Alloys*, Materials Component Engineering Publications Ltd., **1989** pp. 1217–1225.
[30] E. I. Meletis, W. Huang, ibid, pp 1309–1318.
[31] J. G. Craig, R. C. Newman, M. R. Jarret, N. J. Holroyd, G. Champier, B. Dubost, D. Miannay and L. Sabetay (Eds.), *4th Int. Conf. Aluminum Lithium*, J. de Physique, Paris, **1987**, 48, C3: 825–C3: 833.
[32] R. Braun, *Mater. Sci. and Engg.* **1995**, *A190*, 143.
[33] A. Conde, B. J. Fernandoz, J. J. De Damborenea, *Corr. Sci.* **1998**, *40*, 91.
[34] J. B. Lumsden, A. T. Allen, *Corrosion* **1988**, *44*, 527.
[35] A. Conde, J. J. De Damborenea, *Corr. Sci.* **1999**, *41*, 1079.
[36] C. Thakur, R. Balasubramaniam, *Acta Mater.* **1997**, *45*, 1323–13432.
[37] M. Talianker, B. Cina, *Metal. Trans A.* **1989**, *20A*, 2087.
[38] Z. F. Wang, Z. Y. Zhu, Y. Zhang, W. Ke, *Metall Trans A.* **1992**, *23A*, 3337.
[39] J. Garcia, P. Ponthiaux, M. Habashi, J. Galland, G. Champier, B. Dubost, D. Miannay and L. Sabetay, (Eds.), *Proc. 4th Int. Conf. Aluminium Lithium Alloys, J. Phys.* Suppl. **1987**, *48*, pp. C3:861–C3:870.

(Received: April 10, 2006) W 3987
(Final version: April 10, 2006)